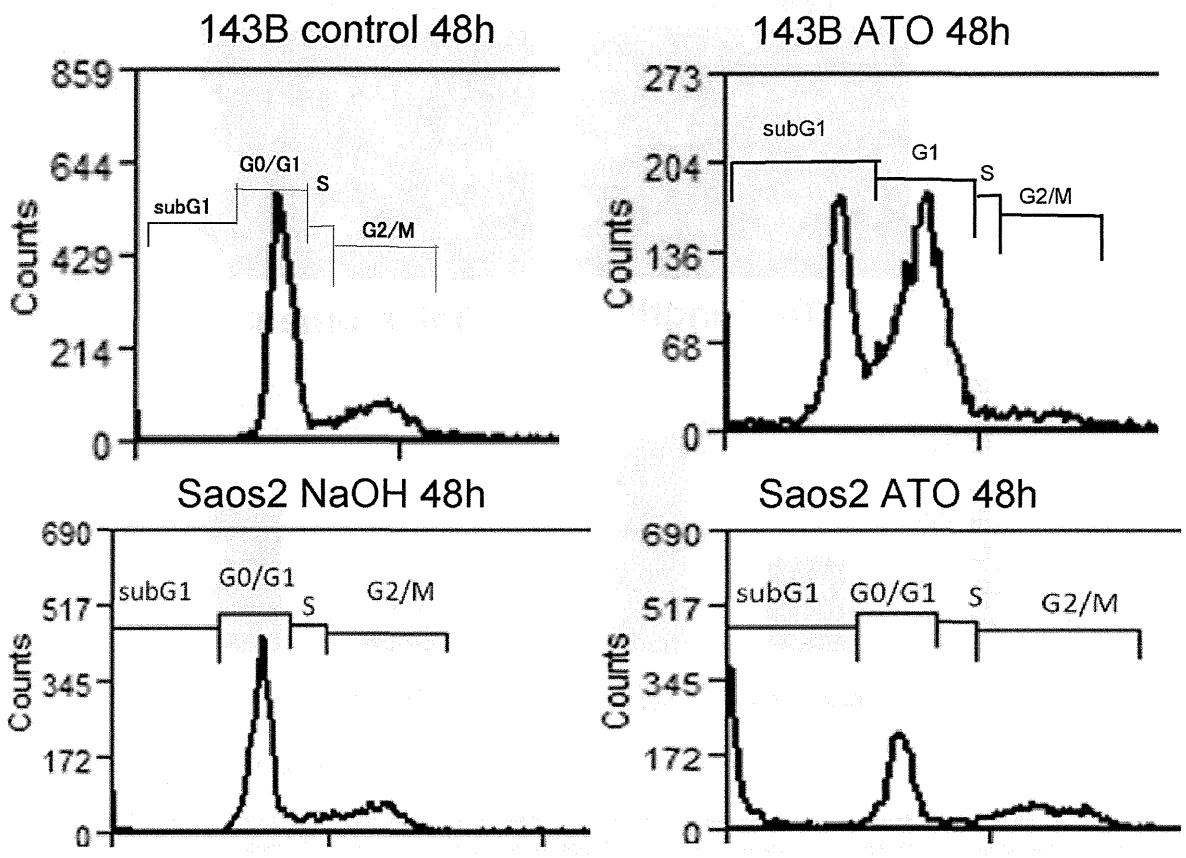

	SubG1	G1	S	G2/M
143B control	1.5±1.6 %	68.7±3.4 %	6.0±1.3 %	23.5±2.4 %
143B (ATO: 3 μM)	24.5±10.0 % **	45.2±21.7 %	2.9±1.1 % **	5.7±2.6 % *
Saos2 control	2.7±2.8 %	56.0±15.3 %	7.4±2.1 %	34.0±10.9 %
Saos2 (ATO: 3 μM)	25.7±6.4 % **	33.0±9.2 %	5.0±3.0 %	24.1±6.0 %

(*: P < 0.01, **: P < 0.05)

Figure 4. ATO promotes apoptotic cell death in human osteosarcoma cells. Human osteosarcoma cells were cultured with or without 1 μM ATO. An equivalent volume of vehicle was used as the control. Flow cytometric analysis was performed after ATO treatment for 48 h. ATO treatment significantly increased the Sub-G1 population of 143B and Saos2 cells. These experiments were performed in triplicate with similar results (*P < 0.01, **P < 0.05).

doi: 10.1371/journal.pone.0069466.g004

signaling promoted the export of CDDP by the ABCG2 transporter and reduced the accumulation of DNA damage in osteosarcoma cells. Inhibition of the Hedgehog pathway by ATO treatment may be useful as an adjunct treatment to conventional chemotherapy for osteosarcoma. In addition, several molecular mechanisms have been reported for inhibition of the Hedgehog pathway by ATO. Kim et al. reported that ATO prevented growth of medulloblastoma by reducing stability of GLI2 protein and ciliary accumulation of GLI2 [25]. Elspeth et al. reported that ATO prevents growth of cancer cell

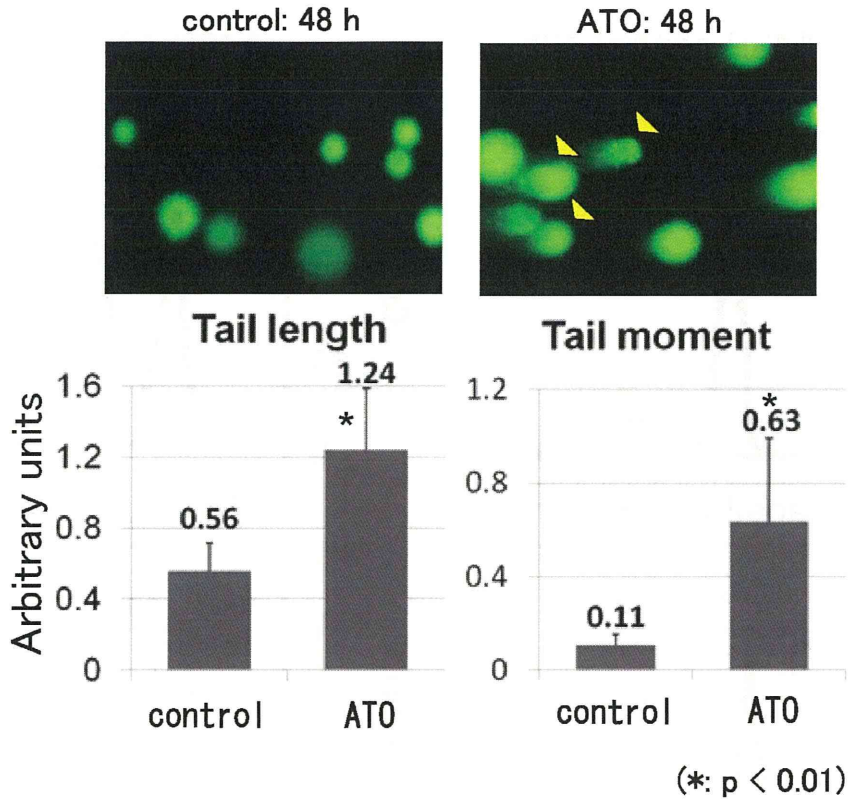

Figure 5. ATO elicits DNA damage in human osteosarcoma. COMET assay was performed to detect DNA damage in single cells after ATO treatment. 143B cells were treated with ATO (3 μM) or an equivalent volume of control vehicle for up to 48 h and analyzed by performing the COMET assay. Graphs represent DNA damage by tail length and tail moment, evaluated as described in the Materials and Methods section. These experiments were performed in triplicate with similar results (*P < 0.01).

doi: 10.1371/journal.pone.0069466.g005

lines and Ewing sarcoma by inhibiting GLI transcription through direct binding to GLI [23]. Although there were some discrepancies related to the mechanism of Hedgehog pathway inhibition by ATO, these studies independently suggest that ATO inhibits malignant tumor growth by inhibition of the Hedgehog pathway at the level of GLI transcription factors. These mechanisms may prevent osteosarcoma growth after ATO treatment. Because aberrant activation of the Hedgehog pathway has been implicated in several malignant tumors, the pharmaceutical industry has invested in the development of Hedgehog pathway inhibitors. SMO inhibitors have been evaluated in recent clinical trials [34,35]. However, treatment with SMO inhibitors showed a lack of efficacy in a portion of patients. Investigation of the underlying mechanism revealed that the patient tumors showed a mutation in SMO that prevented binding of the SMO inhibitors to SMO [15]. Several genes with potential mutations within SMO and downstream of SMO have been found [16–21,36]. In addition, non-Hedgehog pathway-mediated activation of GLI transcription has been reported [37–41]. In this regard, direct GLI inhibition by ATO is likely to be useful for treating tumors with mutations within or downstream of SMO. For example, inhibition of GLI, but not SMO, inhibited tumor growth in myeloid leukemia, colon carcinoma, hepatocellular carcinoma, and osteosarcoma [9,42–44]. Originally, arsenic was used in the 17th century to treat leukemia. ATO has been approved for the treatment of intractable acute promyelocytic leukemia in Japan. Our findings suggest that ATO is one of the most suitable molecular target reagents for inhibiting the Hedgehog pathway in human osteosarcoma. We have now obtained approval from the ethics committee for clinical research, Kagoshima University, to use ATO for treating patients with intractable osteosarcoma.

We examined whether the inhibitory effect of ATO on osteosarcoma growth is mediated, at least in part, by JNK or NF-κB [45–47]. As previously reported, treatment with ATO increased JNK phosphorylation. However, treatment with a JNK inhibitor did not prevent osteosarcoma growth. In contrast, treatment with ATO did not affect NF-κB activation. These

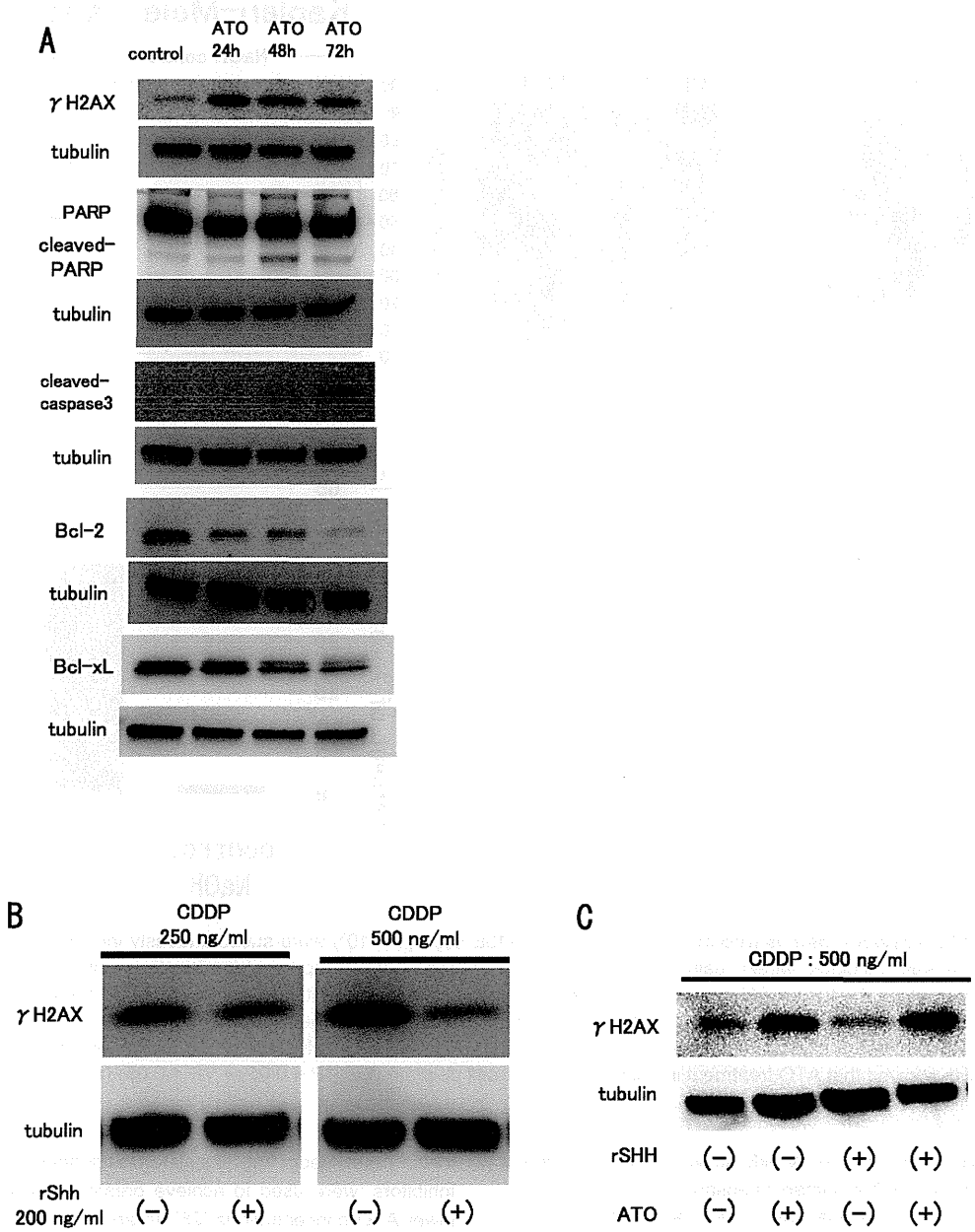

Figure 6. ATO elicits DNA damage and apoptosis. Human osteosarcoma cells were cultured with or without 3 μM ATO. An equivalent volume of vehicle was used as the control. Western blot analysis was performed 48 h and 72 h after ATO treatment. (A) Western blot analysis revealed that ATO treatment increased the protein levels of γH2AX, cleaved PARP, and cleaved caspase-3. ATO treatment decreased the protein levels of Bcl-2 and Bcl-xL. (B) Western blot analysis performed after cisplatin (CDDP) and recombinant human Sonic Hedgehog (rSHH) treatment showed that CDDP treatment upregulated the expression of γH2AX. Addition of Sonic Hedgehog decreased the expression level of γH2AX protein, which was upregulated by CDDP treatment. (C) Western blot analysis was performed following CDDP and recombinant human Sonic Hedgehog (rSHH) or ATO treatment. Addition of Sonic Hedgehog decreased the expression level of γH2AX protein, which was upregulated by CDDP treatment. Addition of ATO restored the γH2AX expression attenuated by rSHH treatment. These experiments were performed in triplicate with similar results.

doi: 10.1371/journal.pone.0069466.g006

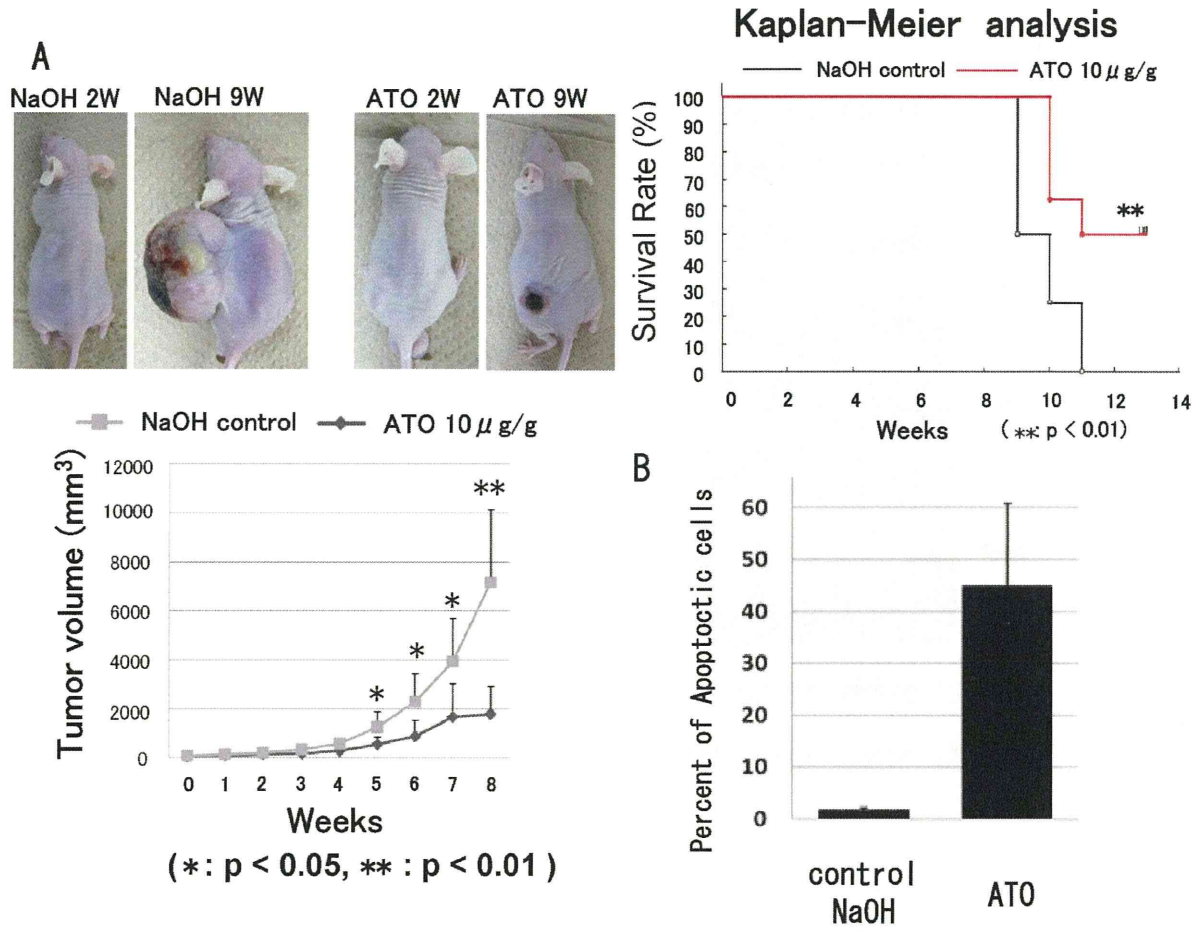

Figure 7. ATO prevents osteosarcoma growth in vivo. 143B cells (1×10^6) were subcutaneously inoculated into nude mice. Tumor volume was calculated weekly using the formula $LW^2/2$ (where L and W represent the length and width of tumors). Seven days after inoculation, the tumor volume was set as 1 and was evaluated at different time points. (A) ATO treatment inhibited tumor growth as compared with control (*P < 0.05 or **P < 0.01) (error bars represent mean [SD]). Kaplan-Meier analysis revealed that ATO treatment provided a significant survival benefit (**P < 0.01). (B) Apoptotic cell death in the tumors was analyzed by TUNEL staining, which showed that ATO treatment increased apoptotic cell death in vivo (*P < 0.05 or **P < 0.05) (error bar indicates SD).

doi: 10.1371/journal.pone.0069466.g007

findings indicate that JNK or NF-κB activation does not affect the cytotoxicity of ATO in human osteosarcoma.

For in vivo examinations, we administered ATO intraperitoneally at 10 mg/kg body weight, as previously reported [25]. Kim et al. examined the ATO levels in mouse sera collected after ATO administration by injection at 10 mg/kg body weight. The peak concentration following intraperitoneal injection at 10 mg/kg was 2.6-fold higher than the peak plasma levels in human patients following intravenous ATO injection at a dose of 0.15 mg/kg body weight [48]. Area under the curve calculations revealed that the total exposure to ATO in mice at the 10 mg/kg dose was 2-fold higher than that in patients. To decrease the ATO concentration, combinations of drugs that inhibit other Hedgehog signaling components, including SMO inhibitors, were used to achieve greater pathway inhibition at lower ATO concentrations [25]. In addition, Kim et al. reported that combined use of ATO and itraconazole, a commonly used antifungal that inhibits SMO by a mechanism distinct from that of cyclopamine and other known SMO antagonists, decreases the dose of ATO and itraconazol required to prevent medulloblastoma and basal cell carcinoma growth associated with acquired resistance to SMO antagonists [24].

In summary, our findings showed that ATO inhibits the Hedgehog pathway and human osteosarcoma cell growth in vitro and in vivo. The combined administration of conventional

anticancer agents or other Hedgehog pathway inhibitors with ATO may be valuable for treating osteosarcoma patients.

Supporting Information

Figure S1. Western blot analysis showed that ATO treatment decreased the expression of phosphorylated JNK. Western blot analysis showed that ATO treatment did not affect the expression levels of NFκB and phosphorylated NFκB proteins. WST assay showed that JNK inhibitor did not affect the proliferation of osteosarcoma cells.

(TIF)

Acknowledgements

We are grateful to Hui Gao for excellent technical assistance.

Author Contributions

Conceived and designed the experiments: TS. Performed the experiments: S. Nakamura S. Nagano HN. Analyzed the data: YI MA TY SK TS. Contributed reagents/materials/analysis tools: MY. Wrote the manuscript: SK TS.

References

1. Sweetnam R (1982) Osteosarcoma. Br J Hosp Med 28: 112: 116-121.
2. Dorfman HD, Czerniak B (1995) Bone cancers. Cancer 75: 203-210. doi:10.1002/1097-0142(19950101)75:1+. PubMed: 8000997
3. Iwamoto Y, Tanaka K, Isu K, Kawai A, Tatezaki S et al. (2009) Multiinstitutional phase II study of neoadjuvant chemotherapy for osteosarcoma (NECO study) in Japan: NECO-93J and NECO-95J. J Orthop Sci 14: 397-404. doi:10.1007/s00776-009-1347-6. PubMed: 19662473.
4. Kager L, Zoubek A, Kastner U, Kempf-Bielack B, Potratz J et al. (2006) Skip metastases in osteosarcoma: experience of the Cooperative Osteosarcoma Study Group. J Clin Oncol 24: 1535-1541. doi:10.1200/JCO.2005.04.2978. PubMed: 16575004.
5. Ingham PW, McMahon AP (2001) Hedgehog signaling in animal development: paradigms and principles. Genes Dev 15: 3059-3087. doi:10.1101/gad.938601. PubMed: 11731473.
6. Ruiz i Altaba A, Sanchez P, Dahmane N (2002) Gli and hedgehog in cancer: tumours, embryos and stem cells. Nat Rev Cancer 2: 361-372.
7. Lum L, Beachy PA (2004) The Hedgehog response network: sensors, switches, and routers. Science 304: 1755-1759. doi:10.1126/science.1098020. PubMed: 15205520.
8. Ruiz i Altaba A, Mas C, Stecca B (2007) The Gli code: an information nexus regulating cell fate, stemness and cancer. Trends Cell Biol 17: 438-447
9. Nagao H, Ijiri K, Hirotsu M, Ishidou Y, Yamamoto T et al. (2011) Role of GLI2 in the growth of human osteosarcoma. J Pathol 224: 169-179. doi:10.1002/path.2880. PubMed: 21506130.
10. Hirotsu M, Setoguchi T, Sasaki H, Matsunoshita Y, Gao H et al. (2010) Smoothened as a new therapeutic target for human osteosarcoma. Mol Cancer 9: 5. doi:10.1186/1476-4598-9-5. PubMed: 20067614.
11. Berman DM, Karhadkar SS, Hallahan AR, Pritchard JI, Eberhart CG et al. (2002) Medulloblastoma growth inhibition by hedgehog pathway blockade. Science 297: 1559-1561. doi:10.1126/science.1073733. PubMed: 12202832.
12. Williams JA, Guicherit OM, Zaharian BI, Xu Y, Chai L et al. (2003) Identification of a small molecule inhibitor of the hedgehog signaling pathway: effects on basal cell carcinoma-like lesions. Proc Natl Acad Sci U S A 100: 4616-4621. doi:10.1073/pnas.0732813100. PubMed: 12679522.
13. Robarge KD, Brunton SA, Castanedo GM, Cui Y, Dina MS et al. (2009) GDC-0449-a potent inhibitor of the hedgehog pathway. Bioorg Med Chem Lett 19: 5576-5581. doi:10.1016/j.bmcl.2009.08.049. PubMed: 19716296.
14. Tremblay MR, Lescarbeau A, Grogan MJ, Tan E, Lin G et al. (2009) Discovery of a potent and orally active hedgehog pathway antagonist (IPI-926). J Med Chem 52: 4400-4418. doi:10.1021/jm900305z. PubMed: 19522463.
15. Rudin CM, Hann CL, Laterra J, Yauch RL, Callahan CA et al. (2009) Treatment of medulloblastoma with hedgehog pathway inhibitor GDC-0449. N Engl J Med 361: 1173-1178. doi:10.1056/NEJMoa0902903. PubMed: 19726761.
16. Xie J, Murone M, Luoh SM, Ryan A, Gu Q et al. (1998) Activating Smoothened mutations in sporadic basal-cell carcinoma. Nature 391: 90-92. doi:10.1038/34201. PubMed: 9422511.
17. Taipale J, Chen JK, Cooper MK, Wang B, Mann RK et al. (2000) Effects of oncogenic mutations in Smoothened and Patched can be reversed by cyclopamine. Nature 406: 1005-1009. doi: 10.1038/35023008. PubMed: 10984056.
18. Taylor MD, Liu L, Raffel C, Hui CC, Mainprize TG et al. (2002) Mutations in SUFU predispose to medulloblastoma. Nat Genet 31: 306-310. doi:10.1038/ng916. PubMed: 12068298.
19. Tostar U, Malm CJ, Meis-Kindblom JM, Kindblom LG, Toftgård R et al. (2006) Deregulation of the hedgehog signalling pathway: a possible role for the PTCH and SUFU genes in human rhabdomyoma and rhabdomyosarcoma development. J Pathol 208: 17-25. doi:10.1002/path.1882. PubMed: 16294371.
20. Lee Y, Kawagoe R, Sasai K, Li Y, Russell HR et al. (2007) Loss of suppressor-of-fused function promotes tumorigenesis. Oncogene 26: 6442-6447. doi:10.1038/sj.onc.1210467. PubMed: 17452975.
21. Sheng T, Li C, Zhang X, Chi S, He N et al. (2004) Activation of the hedgehog pathway in advanced prostate cancer. Mol Cancer 3: 29. doi: 10.1186/1476-4598-3-29. PubMed: 15482598.
22. Lengfelder E, Hofmann WK, Nowak D (2012) Impact of arsenic trioxide in the treatment of acute promyelocytic leukemia. Leukemia 26: 433-442. doi:10.1038/leu.2011.245. PubMed: 21904379.
23. Beauchamp EM, Ringer L, Bulut G, Sajwan KP, Hall MD et al. (2011) Arsenic trioxide inhibits human cancer cell growth and tumor development in mice by blocking Hedgehog/GLI pathway. J Clin Invest 121: 148-160. doi:10.1172/JCI42874. PubMed: 21183792.
24. Kim J, Aftab BT, Tang JY, Kim D, Lee AH et al. (2013) Itraconazole and arsenic trioxide inhibit Hedgehog pathway activation and tumor growth associated with acquired resistance to smoothened antagonists. Cancer Cell 23: 23-34. doi:10.1016/j.ccr.2012.11.017. PubMed: 23291299.
25. Kim J, Lee JJ, Kim J, Gardner D, Beachy PA (2010) Arsenic antagonizes the Hedgehog pathway by preventing ciliary accumulation and reducing stability of the Gli2 transcriptional effector. Proc Natl Acad Sci U S A 107: 13432-13437. doi:10.1073/pnas.1006822107. PubMed: 20624968.
26. Plesca D, Crosby ME, Gupta D, Almasan A (2007) E2F4 function in G2: maintaining G2-arrest to prevent mitotic entry with damaged DNA. Cell Cycle 6: 1147-1152. doi:10.4161/cc.6.10.4259. PubMed: 17507799.
27. Jung HS, Kim HS, Lee MJ, Shin HY, Ahn HS et al. (2006) Arsenic trioxide concentration determines the fate of Ewing's sarcoma family tumors and neuroblastoma cells in vitro. FEBS Lett 580: 4969-4975. doi:10.1016/j.febslet.2006.07.077. PubMed: 16930595.
28. Mathieu J, Besançon F (2006) Clinically tolerable concentrations of arsenic trioxide induce p53-independent cell death and repress NF-kappa B activation in Ewing sarcoma cells. Int J Cancer 119: 1723-1727. doi:10.1002/ijc.21970. PubMed: 16646077.
29. Yang W, Liu X, Choy E, Mankin H, Hornicek FJ et al. (2012) Targeting hedgehog-GLI-2 pathway in osteosarcoma. J Orthop Res, 31: 502–9. PubMed: 22968906.
30. Bigelow RL, Chari NS, Unden AB, Spurgers KB, Lee S et al. (2004) Transcriptional regulation of bcl-2 mediated by the sonic hedgehog signaling pathway through gli-1. J Biol Chem 279: 1197-1205. PubMed: 14555646.
31. Regl G, Kasper M, Schnidar H, Eichberger T, Neill GW et al. (2004) Activation of the BCL2 promoter in response to Hedgehog/GLI signal transduction is predominantly mediated by GLI2. Cancer Res 64: 7724-7731. doi:10.1158/0008-5472.CAN-04-1085. PubMed: 15520176.
32. Narita S, So A, Ettinger S, Hayashi N, Muramaki M et al. (2008) GLI2 knockdown using an antisense oligonucleotide induces apoptosis and chemosensitizes cells to paclitaxel in androgen-independent prostate cancer. Clin Cancer Res 14: 5769-5777. doi: 10.1158/1078-0432.CCR-07-4282. PubMed: 18794086.

33. Singh RR, Kunkalla K, Qu C, Schlette E, Neelapu SS et al. (2011) ABCG2 is a direct transcriptional target of hedgehog signaling and involved in stroma-induced drug tolerance in diffuse large B-cell lymphoma. Oncogene 30: 4874-4886. doi:10.1038/onc.2011.195. PubMed: 21625222.
34. Von Hoff DD, LoRusso PM, Rudin CM, Reddy JC, Yauch RL et al. (2009) Inhibition of the hedgehog pathway in advanced basal-cell carcinoma. N Engl J Med 361: 1164-1172. doi:10.1056/NEJMoa0905360. PubMed: 19726763.
35. Bisht S, Brossart P, Maitra A, Feldmann G (2010) Agents targeting the Hedgehog pathway for pancreatic cancer treatment. Curr Opin Investig Drugs 11: 1387-1398. PubMed: 21154121.
36. Chen JK, Taipale J, Young KE, Maiti T, Beachy PA (2002) Small molecule modulation of Smoothened activity. Proc Natl Acad Sci U S A 99: 14071-14076. doi:10.1073/pnas.182542899. PubMed: 12391318.
37. Roberts WM, Douglass EC, Peiper SC, Houghton PJ, Look AT (1989) Amplification of the gli gene in childhood sarcomas. Cancer Res 49: 5407-5413. PubMed: 2766305.
38. Khatib ZA, Matsushime H, Valentine M, Shapiro DN, Sherr CJ et al. (1993) Coamplification of the CDK4 gene with MDM2 and GLI in human sarcomas. Cancer Res 53: 5535-5541. PubMed: 8221695.
39. Zwerner JP, Joo J, Warner KL, Christensen L, Hu-Lieskovan S et al. (2008) The EWS/FLI1 oncogenic transcription factor deregulates GLI1. Oncogene 27: 3282-3291. doi:10.1038/sj.onc.1210991. PubMed: 18084326.
40. Beauchamp E, Bulut G, Abaan O, Chen K, Merchant A et al. (2009) GLI1 is a direct transcriptional target of EWS-FLI1 oncoprotein. J Biol Chem 284: 9074-9082. doi:10.1074/jbc.M806233200. PubMed: 19189974.
41. Nolan-Stevaux O, Lau J, Truitt ML, Chu GC, Hebrok M et al. (2009) GLI1 is regulated through Smoothened-independent mechanisms in neoplastic pancreatic ducts and mediates PDAC cell survival and transformation. Genes Dev 23: 24-36. doi:10.1101/gad.1753809. PubMed: 19136624.
42. Xu Y, Chenna V, Hu C, Sun HX, Khan M et al. (2011) Polymeric nanoparticle-encapsulated hedgehog pathway inhibitor HPI-1 (NanoHHI) inhibits systemic metastases in an orthotopic model of human hepatocellular carcinoma. Clin Cancer Res 18: 1291-1302. PubMed: 21868763.
43. Pan D, Li Y, Li Z, Wang Y, Wang P et al. (2012) Gli inhibitor GANT61 causes apoptosis in myeloid leukemia cells and acts in synergy with rapamycin. Leuk Res 36: 742-748. doi:10.1016/j.leukres.2012.02.012. PubMed: 22398221.
44. Mazumdar T, Devecchio J, Agyeman A, Shi T, Houghton JA (2011) Blocking Hedgehog survival signaling at the level of the GLI genes induces DNA damage and extensive cell death in human colon carcinoma cells. Cancer Res 71: 5904-5914. doi: 10.1158/0008-5472.CAN-10-4173. PubMed: 21747117.
45. Giafis N, Katsoulidis E, Sassano A, Tallman MS, Higgins LS et al. (2006) Role of the p38 mitogen-activated protein kinase pathway in the generation of arsenic trioxide-dependent cellular responses. Cancer Res 66: 6763-6771. doi:10.1158/0008-5472.CAN-05-3699. PubMed: 16818652.
46. Cavigelli M, Li WW, Lin A, Su B, Yoshioka K et al. (1996) The tumor promoter arsenite stimulates AP-1 activity by inhibiting a JNK phosphatase. EMBO J 15: 6269-6279. PubMed: 8947050.
47. Kapahi P, Takahashi T, Natoli G, Adams SR, Chen Y et al. (2000) Inhibition of NF-kappa B activation by arsenite through reaction with a critical cysteine in the activation loop of Ikappa B kinase. J Biol Chem 275: 36062-36066. doi:10.1074/jbc.M007204200. PubMed: 10967126.
48. Shen ZX, Chen GQ, Ni JH, Li XS, Xiong SM et al. (1997) Use of arsenic trioxide (As2O3) in the treatment of acute promyelocytic leukemia (APL): II. Clinical efficacy and pharmacokinetics in relapsed patients. Blood 89: 3354-3360. PubMed: 9129042.

Cell Biology:

Human Immunodeficiency Virus Type 1 Enhancer-binding Protein 3 Is Essential for the Expression of Asparagine-linked Glycosylation 2 in the Regulation of Osteoblast and Chondrocyte Differentiation

Katsuyuki Imamura, Shingo Maeda, Ichiro Kawamura, Kanehiro Matsuyama, Naohiro Shinohara, Yuhei Yahiro, Satoshi Nagano, Takao Setoguchi, Masahiro Yokouchi, Yasuhiro Ishidou and Setsuro Komiya

J. Biol. Chem. 2014, 289:9865-9879.
doi: 10.1074/jbc.M113.520585 originally published online February 21, 2014

THE JOURNAL OF BIOLOGICAL CHEMISTRY VOL. 289, NO. 14, pp. 9865–9879, April 4, 2014

Human Immunodeficiency Virus Type 1 Enhancer-binding Protein 3 Is Essential for the Expression of Asparagine-linked Glycosylation 2 in the Regulation of Osteoblast and Chondrocyte Differentiation*[S]

Received for publication, September 20, 2013, and in revised form, January 26, 2014 Published, JBC Papers in Press, February 21, 2014, DOI 10.1074/jbc.M113.520585

Katsuyuki Imamura[‡§], Shingo Maeda[‡1], Ichiro Kawamura[§], Kanehiro Matsuyama[‡§], Naohiro Shinohara[‡§], Yuhei Yahiro[‡§], Satoshi Nagano[§], Takao Setoguchi[¶], Masahiro Yokouchi[§], Yasuhiro Ishidou[‡], and Setsuro Komiya[‡§¶]

From the Departments of [‡]Medical Joint Materials and [§]Orthopaedic Surgery and the [¶]Near-Future Locomotor Organ Medicine Creation Course, Graduate School of Medical and Dental Sciences, Kagoshima University, Kagoshima 890-8544, Japan

Background: The mechanisms by which Hivep3 regulates the osteochondrogenesis remain elusive.
Results: Knockdown of Hivep3 down-regulated *Alg2* expression. Alg2 suppressed osteoblast differentiation by inhibiting the activity of Runx2. Alg2 silencing suppressed the expression of *Creb3l2* and chondrogenesis.
Conclusion: Alg2 may be a modulator of osteochondrogenesis.
Significance: This is the first report to describe the association of an Alg gene with osteochondrogenesis.

Human immunodeficiency virus type 1 enhancer-binding protein 3 (*Hivep3*) suppresses osteoblast differentiation by inducing proteasomal degradation of the osteogenesis master regulator Runx2. In this study, we tested the possibility of cooperation of Hivep1, Hivep2, and Hivep3 in osteoblast and/or chondrocyte differentiation. Microarray analyses with ST-2 bone stroma cells demonstrated that expression of any known osteochondrogenesis-related genes was not commonly affected by the three Hivep siRNAs. Only *Hivep3* siRNA promoted osteoblast differentiation in ST-2 cells, whereas all three siRNAs cooperatively suppressed differentiation in ATDC5 chondrocytes. We further used microarray analysis to identify genes commonly down-regulated in both MC3T3-E1 osteoblasts and ST-2 cells upon knockdown of *Hivep3* and identified asparagine-linked glycosylation 2 (*Alg2*), which encodes a mannosyltransferase residing on the endoplasmic reticulum. The *Hivep3* siRNA-mediated promotion of osteoblast differentiation was negated by forced Alg2 expression. Alg2 suppressed osteoblast differentiation and bone formation in cultured calvarial bone. Alg2 was immunoprecipitated with Runx2, whereas the combined transfection of Runx2 and Alg2 interfered with Runx2 nuclear localization, which resulted in suppression of Runx2 activity. Chondrocyte differentiation was promoted by Hivep3 overexpression, in concert with increased expression of *Creb3l2*, whose gene product is the endoplasmic reticulum stress transducer crucial for chondrogenesis. *Alg2* silencing suppressed *Creb3l2* expression and chondrogenesis of ATDC5 cells, whereas infection of Alg2-expressing virus promoted chondrocyte maturation in cultured cartilage rudiments. Thus, Alg2, as a downstream mediator of Hivep3, suppresses osteogenesis, whereas it promotes chondrogenesis. To our knowledge, this study is the first to link a mannosyltransferase gene to osteochondrogenesis.

In skeletal development and bone remodeling, osteoblasts play major roles not only in bone formation but also in inducing the differentiation of bone-resorbing osteoclasts (1, 2). Runx2 is a critical transcription factor in osteoblast differentiation, as evidenced by Runx2 knock-out mice, which exhibit a complete lack of both intramembranous and endochondral ossification due to the absence of osteoblasts (3). Cleidocranial dysplasia, a human autosomal dominant inherited disorder of bone development, is characterized by hypoplasia of clavicles and abnormalities in cranial and facial bones and is caused by mutations in the *Runx2* gene (4, 5). Some genes, *e.g.* LDL receptor-related protein 5 (*Lrp5*), sclerostin (*Sost*), and human immunodeficiency virus type 1 enhancer-binding protein 3 (*Hivep3*), have been found to control osteoblast function in the adult human and/or mouse during postnatal skeletal remodeling (6–10).

Hivep3, also known as Schnurri-3, Zas3, and Krc, is a member of three mammalian homologs of the Hivep/Schnurri family of large zinc finger proteins. Hivep proteins have been studied for their roles in the regulation of an assortment of genes, including those encoding collagen type IIA, αA-crystallin, β-interferon, and HIV genes (11). Hivep2 can indirectly interact with the peroxisome proliferator-activated receptor γ2 (*Pparg2*) promoter to promote adipogenesis, through binding to Smad1, an intracellular mediator of bone morphogenetic protein (BMP)[2] signaling. Hivep2 can also dock to CCAAT/enhancer-binding protein α (C/ebpα) to interact

* This work was supported by Japan Society for the Promotion of Science KAKENHI Grants 23592221 (to S. M.) and 23592222 (to Y. I.), a grant from the Cell Science Research Foundation (to S. M.), and a grant from the Hip Joint Foundation of Japan (to S. M.).
[S] This article contains supplemental Tables 1–5.
[1] To whom correspondence should be addressed: Dept. of Medical Joint Materials, Graduate School of Medical and Dental Sciences, Kagoshima University, 8-35-1 Sakuragaoka, Kagoshima 890-8544, Japan. Tel.: 81-99-275-5381; Fax: 81-99-265-4699; E-mail: maeda-s@umin.ac.jp or s-maeda@m3.kufm.kagoshima-u.ac.jp.

[2] The abbreviations used are: BMP, bone morphogenetic protein; ER, endoplasmic reticulum; ALP, alkaline phosphatase; ECM, extracellular matrix; CDG, congenital disorders of glycosylation; qRT, quantitative RT; ALG, asparagine-linked glycosylation.

with a CCAAT site on the distal part of the *Pparg* gene (12). Mice lacking Hivep3 demonstrate adult-onset osteosclerosis with increased bone volume due to enhanced osteoblast activity (10). Hivep3 promotes proteasomal degradation of the Runx2 protein through recruitment of the E3 ubiquitin ligase Wwp1 to Runx2 (10). A D-domain motif within Hivep3 mediates the interaction with and inhibition of ERK mitogen-activated protein kinase (MAPK), thereby inhibiting Wnt/Lrp5 signaling through regulation of the activity of a downstream mediator glycogen synthase kinase 3-β (Gsk3β). This interaction results in the suppression of subsequent osteoblast differentiation (13). In addition, Hivep3 indirectly promotes osteoclastogenesis by promoting osteoblastic expression of receptor activator of nuclear factor-κB ligand (Rankl), a crucial factor for osteoclast differentiation (14). Hivep3 also cell-autonomously promotes osteoclastogenesis by inducing the expression of *Nfatc1*, a master transcription factor in osteoclast differentiation, by interacting with Traf6 to enhance its activity while forming a complex with c-Jun to activate the *Nfatc1* promoter (15). Thus, Hivep3 controls both bone formation and resorption at multiple steps to maintain normal bone mass. However, whether Hivep3 controls gene expression in osteoblasts to regulate osteoblast activity is unclear.

In contrast to *Hivep3* knock-out mice, mice lacking *Hivep2* exhibited decreased cortical bone volume and increased cancellous bone mass (16), suggesting different roles for Hivep2 and Hivep3 in the skeleton. Combined ablation of *Hivep2* and *Hivep3* in mice resulted in synergistically increased trabecular bone volume, demonstrating a redundancy between the two proteins in the regulation of postnatal bone mass (17). Interestingly, in the double knock-out mice, the growth plate cartilage of the long bones was uncoupled with bone phenotype, with significantly delayed maturation of chondrocytes resulting in chondrodysplasia (17), suggesting a role for Hivep proteins in the promotion of chondrocyte differentiation. However, the mechanism by which Hivep proteins affect chondrogenesis remains unknown. In addition, to date, no information has been reported on the possible role of Hivep1 in osteogenesis and/or chondrogenesis.

In this study, *in vitro* analysis showed that, among the three Hivep proteins, only Hivep3 was inhibitory and that the others promoted osteoblast differentiation. In contrast, all three Hivep genes seemed to support chondrocyte differentiation in BMP-2-induced ATDC5 cells, suggesting their redundancy in chondrogenesis. We found that asparagine-linked glycosylation 2 (*Alg2*) is commonly down-regulated in BMP-2-induced osteoblast differentiation in both MC3T3-E1 and ST-2 cells. Alg2 inhibited Runx2 activity without altering its protein level, resulting in suppression of osteoblast differentiation. Interestingly, in chondrogenesis of ATDC5 cells, Hivep3 induced the expression of cAMP-responsive element binding-protein 3-like 2 (*Creb3l2*), an endoplasmic reticulum (ER) stress transducer crucial for chondrogenesis (18), suggesting a possible role for Hivep3 in physiological mild ER stress. Alg2 was also decreased by *Hivep3* knockdown in ATDC5 chondrocytes, whereas silencing of Alg2 suppressed the expression of *Creb3l2* and chondrogenesis. To our knowledge, this study is the first to show a linkage between an asparagine-linked glycosylation mannosyltransferase gene and osteochondrogenesis.

EXPERIMENTAL PROCEDURES

Cell Culture and Differentiation—The mouse calvarial bone-derived osteoblast cell line, MC3T3-E1 (clone 4), and the mouse chondrogenic fibroblast cell line, C3H10T1/2, were obtained from the ATCC. The mouse bone marrow stromal cell line ST-2 and the mouse chondrogenic cell line ATDC5 were obtained from the RIKEN BioResource Center. MC3T3-E1 cells were cultured in minimum essential medium α (Invitrogen) containing 10% fetal bovine serum (FBS). ST-2 cells were cultured in RPMI 1640 medium (Sigma) containing 10% FBS. ATDC5 cells were cultured in Dulbecco's modified Eagle's medium (DMEM)/Ham's F-12 (1:1) (Invitrogen) containing 5% FBS. C3H10T1/2 cells were cultured in basal medium Eagle's (Sigma) with 2 mM L-glutamine and 10% FBS. COS-7 cells were purchased from RIKEN BioResource Center and maintained in DMEM supplemented with 10% FBS. All cell culture medium contained 100 units/ml penicillin G and 100 μg/ml streptomycin. Cell differentiation was induced by the addition of recombinant human BMP-2 (PeproTech) at a concentration of 300 ng/ml. Micromass culture of ATDC5 cells was performed as described previously (19) to accelerate the maturation of chondrocyte differentiation.

Alkaline Phosphatase (ALP) and Alcian Blue Staining—The activity of ALP secreted into the extracellular matrix (ECM) of cultured cells was visualized with an ALP staining kit (85L-3R, Sigma). Cartilaginous glycosaminoglycans produced in the ECM by cultured cells were stained with Alcian blue 8GX (Sigma).

RNA Interference—Dharmacon siRNA ON-TARGETplus SMARTpool, a mixture of four independent siRNAs against mouse *Hivep1*, *Hivep2*, *Hivep3*, and *Alg2*, and the control reagent were purchased from Thermo Scientific. siRNAs were transfected into cells using Lipofectamine RNAiMax (Invitrogen).

Real Time Quantitative PCR—Cells were lysed with TRIzol reagent (Invitrogen) to purify RNA, and 1 μg of total RNA was subjected to reverse transcription with the Verso cDNA kit (Thermo Scientific). The relative amounts of the gene transcripts were determined by real time quantitative PCR using SYBR premix Ex TaqII (Takara) and the Thermal Cycler Dice TP850 system (Takara). PCRs were performed in duplicate per sample, and the measured expression level of each gene was normalized to that of *Hprt1*. The sequence information for the primers used is listed in supplemental Table 1. All primer sets are for mouse genes, except for the m/h*Hivep3* primer set, which can be used to amplify both the mouse and human *Hivep3* genes. For evaluation of the tissue distribution of the Hivep genes and Alg2 *in vivo*, tissues were harvested from 3-month-old mice, and mRNA was purified with TRIzol reagent before subjecting samples to qRT-PCR.

Microarray Analysis—Cells transfected with siRNA overnight were further incubated with BMP-2 for 2 days before being lysed with TRIzol reagent for mRNA purification. mRNA samples were cleaned up using the RNeasy MinElute Cleanup kit (Qiagen) and analyzed on a Mouse Gene 2.0 ST Array (Affymetrix) by BioMatrix Research.

Plasmids, Adenovirus, and Lentivirus—The mouse Hivep3 expression plasmid, pEF-Shn3, was a kind gift from Dr. Laurie Glimcher (Harvard Medical School). The human HIVEP3 expression plasmid pFN21A-HIVEP3 was obtained from Kazusa DNA Research Institute. The mouse type II Runx2 expression plasmid was a kind gift from Dr. Toshihisa Komori (Nagasaki University). The FLAG-Runx2-def expression plasmid has been described in our previous study (20). Mouse *Alg2* or *Runx2* cDNA was cloned from ST-2 cells by using a RT-PCR-based technique, subcloned into the entry vector, pENTR, and further transferred into the C-terminally V5-tagged expression vector, pEF-DEST51 (Invitrogen). For overexpression assays, cells were transfected with expression vectors using FuGENE 6 (Roche Applied Science) or Lipofectamine 2000 (Invitrogen). Cells transiently expressing the transgenes were selected and enriched by incubation with G418 disulfate (Nacalai Tesque) at a concentration of 250 μg/ml for 3–7 days. To generate adenovirus-carrying *Alg2* cDNA, the *Alg2* gene in the pENTR-Alg2 vector was transferred into the C-terminally V5-tagged adenovirus expression vector pAd/CMV/V5-DEST by LR recombination (Invitrogen) and was further transfected into the adenovirus-producing cell line 293A according to the manufacturer's protocol. The pAd/CMV/V5-GW/lacZ adenovirus expression vector was used to generate a control adenovirus. For generation of lentivirus carrying the *Alg2* gene, pENTR-Alg2 and pENTR-5′EF1αP were subjected to LR recombination with pLenti6.4/R4R2/V5-DEST (Invitrogen) to generate a lentiviral vector expressing C-terminally V5-tagged Alg2 from the EF1α promoter. The lentiviral expression vector or pLenti6/V5/GW-lacZ control vector was transfected into 293FT cells to generate the lentivirus. Virus infection into ST-2 cells was performed at a multiplicity of infection of 100. Cells infected with the lentivirus were selected by treatment with blasticidin S HCl (Invitrogen) at a concentration of 2.5 μg/ml. These experiments were approved by the Kagoshima University safety control committee for gene recombination techniques (number 22053).

Embryonic Bone Organ Culture—Calvarial bone and metatarsal bone (cartilage) rudiments were harvested from C57BL/6J mouse embryos at 17.5 days post-coitum (E17.5) and cultured in minimum essential medium α or DMEM/Ham's F-12 (1:1), respectively, supplemented with 10% FBS, 100 units/ml penicillin G, and 100 μg/ml streptomycin, as described (21). The bone rudiments were incubated in virus solution overnight for infection of adenovirus or lentivirus. Cultured bones and cartilages were fixed in 96% ethanol and stained with 0.015% Alcian blue 8GX in a mixture solution of 96% ethanol/acetic acid (4:1) for 1 day, followed by a dehydration step in 100% ethanol. Dehydrated bones were immersed briefly in 1% potassium hydroxide (KOH), followed by staining in 0.001% alizarin red S (Sigma) in 1% KOH for 1 day. Images were captured with stereomicroscope M165FC (Leica). The animal experiments were approved by the Institutional Animal Care and Use Committee of Kagoshima University (number MD12137).

Immunoprecipitation and Immunoblotting—For immunoprecipitation assays, COS-7 cells were transfected with Alg2-V5 and/or FLAG-Runx2 plasmids and were lysed in M-PER lysis buffer (Thermo Scientific) supplemented with aprotinin and phenylmethylsulfonyl fluoride (PMSF). The lysate was immunoprecipitated with anti-FLAG M2-agarose affinity gel (A2220, Sigma), and the M2 antibody-bound protein complex was eluted by incubation with 3×FLAG peptide (F4799, Sigma), according to the manufacturer's protocol. For immunoblotting assays, cells were lysed in either M-PER or NE-PER lysis buffer (Thermo Scientific) supplemented with aprotinin and PMSF or directly with 1× SDS sample buffer. SDS-PAGE, membrane transfer, and chemiluminescence were performed using a standard protocol. The blots were incubated with primary antibodies against Alg2 (1:1000; LS-C81338, Lifespan Biosciences), Runx2 (1:200; M-70, sc-10758, Santa Cruz Biotechnology), Runx2 (1:1000; 8G5, MBL), Sp7 (1:1000, ab22552, Abcam), Ibsp (1:1000, LS-C190916, Lifespan Biosciences), type II collagen (1:1000, LS-C175971, Lifespan Biosciences), Creb3l2 (1:1000, ab76856, Abcam), V5 (1:5000; R960-25, Invitrogen), FLAG (1:1000; M2, F1804, Sigma), and tubulin (1:1000; DM1A, T9026, Sigma) and with horseradish peroxidase (HRP)-conjugated anti-rabbit and anti-mouse secondary antibodies (1:10,000) (Cell Signaling). For examination of half-life of Runx2 protein, after overnight transfection with siRNA of *Hivep3*, ST-2 cells were treated with cycloheximide (Sigma) at 100 μg/ml, followed by immunoblotting using anti-Runx2 antibody. Signals were detected using the LAS 4000 mini image analyzer (Fujifilm).

Immunofluorescence—For immunofluorescence assays, cells transfected with Runx2 and/or Alg2-V5 expression plasmids were fixed with 4% paraformaldehyde in PBS for 30 min and treated with 0.2% Triton X-100. CAS block (Zymed Laboratories Inc.) was used for blocking. Cells were incubated with anti-Runx2 (1:100; 8G5, MBL), Alexa Fluor 568 rabbit anti-mouse IgG (1:1000; A11061, Invitrogen), and anti-V5-FITC (1:500; R619-25, Invitrogen) antibodies. Nuclei were stained with Hoechst dye (Invitrogen). Confocal fluorescent imaging was performed and analyzed using a laser scanning microscope system (LSM 700, Zeiss). For confirmation of the efficiency of virus infection in cultured bones, formalin-fixed mouse E17.5 embryo calvariae or metatarsal bones were embedded in paraffin blocks, which were sliced at a 4-μm thickness. The antigen was retrieved by Liberate Antibody Binding (L.A.B.) solution (Polysciences). A CAS block was used for blocking. Bone sections were incubated with anti-V5-FITC antibody. Images were captured with microscope AX80 and digital camera DP70 (Olympus).

Luciferase Assay—COS-7 cells or ST-2 cells were seeded in triplicate in 24-well plates and transiently transfected with the 6×OSE2 luciferase reporter plasmid (a kind gift from Dr. Toshihisa Komori), the mutant 6×OSE2 luciferase reporter plasmid (a kind gift from Dr. Gerard Karsenty, Columbia University Medical Center), the pGL4.75hRlucCMV *Renilla* vector (Promega), and expression vectors for Runx2, Alg2, or Hivep3. Dual-Luciferase assays were performed as described earlier (20) by using the GloMax 96 microplate luminometer (Promega).

Statistical Analysis—The data in this study have been expressed as mean ± S.D. values of three independent experiments. Statistical comparisons between the different treatments were performed using an unpaired Student's *t* test in